

# Flow Instability of Silicon Melt in Magnetic Fields

Koichi Kakimoto<sup>1</sup> and Lijun Liu<sup>1</sup>

**Abstract:** This paper deals with the investigation of the flow instability of molten silicon in a magnetic field during crystal growth by means of the Czochralski method. The flow exhibits a three-dimensional structure due to a transverse non-axisymmetric pattern of the magnetic field. The melt-crystal interface is found to be nearly two-dimensional. The azimuthal non-uniformity of the temperature field is much weaker on the crystal and crucible sidewalls in the case of high rotation rates of crucible and crystal than in the case of non-rotating crucible and crystal.

**keyword:** Magnetic fields, Computer simulation, Global modeling, Czochralski method, Semiconductor silicon.

## 1 Introduction

Bulk crystalline silicon with high-quality has become an essential material for information society. The distribution of temperature in the crystal during growth affects the distribution of vacancy and formation of voids in the crystal. Therefore, it is important to control temperature distribution in a crystal through melt flow control. Along these lines, there have been many studies on the instabilities of melt convection and related control strategies [see, e.g., Amberg and Shiomi (2005); Gelfgat et al. (2005); Lappa (2005); Lan and Yeh (2005); Li et al. (2006); Tsukada et al. (2005); Sohail and Saghir (2006); Jaber and Saghir (2006)].

The magnetic-field applied CZ-Si crystal growth method (MCZ) is an effective method for controlling such flows. This technique can modify the shape of melt-crystal interface as it directly influences convection in the melt. A method traditionally used for flow control and commercial production, in particular, foresees a "transverse" magnetic fields (it is usually referred to as transverse-magnetic-field applied Czochralski method - TMCZ). Many research works [Grabner et al. (2001); Hirata and Hoshikawa (1989); Kakimoto et al. (1996); Kakimoto

and Ozoe (2000); Kakimoto (2002); Kakimoto et al. (2002); Krause et al. (2004); Ozoe and Iwamoto (1994); Sabhapathy and Salcudean (1991); Liu et al. (2005)] regarding the TMCZ have been published in the literature. It is worth noting, however, that most of the numerical studies on CZ-Si growth with a transverse magnetic field have been limited to the three-dimensional melt flow in a crucible by imposing a flat melt-crystal interface with assigned external thermal boundary conditions.

However, since the real shape of the melt-crystal interface and the thermal field near it are of great interest for commercial use, three-dimensional (3D) global modeling that takes into account the high degree of non-linearity of the growth system, the inherent three-dimensionality of the melt flow and thermal field under the influence of a transverse magnetic field is necessary. Therefore, one of our aims in this study is the determination of the effects of a transverse magnetic field on the melt-crystal interface by using our recently developed 3D global model [Liu and Kakimoto (2005)]. Moreover, we focus on the melt flow instability.

## 2 3D modeling

The geometry of the investigated CZ furnace has an axisymmetric structure with the exception of the melt-crystal interface, which might be three-dimensional in space. The growth system is assumed to be quasi-steady since the crystal growth rate is small (about 1mm/min). The constituents of the furnace are subdivided into several block regions. Each of these blocks is covered with a structured grid. In order to perform 3D global modeling with moderate requirements of computer memory and computation time, a mixed 2D/3D space discretization scheme was developed in the 3D global model [Liu and Kakimoto (2005)]. By using this scheme, the components in the central region of the furnace, namely, the 3D domain, are discretized in a three-dimensional configuration, while the domains away from the core region, namely, the 2D domain, are discretized in a two-dimensional configuration. This is based on the fact that

<sup>1</sup> Kyushu University, Kasuga, Fukuoka, JAPAN

the three-dimensionality of the system is induced originally in the melt flow.

In this study, the 3D domain includes the crystal, the melt and the crucible, while the other regions in the furnace are included in the 2D domain. Liu and Kakimoto (2005) demonstrated that in this small furnace the non-uniformity of the thermal field in the azimuthal direction is negligible in the heater.

The melt flow is solved with a Reynolds-averaged Navier-Stokes solver. The crucible, ambient gas and crystal puller are electrically insulated. The computation domain related to the electromagnetic field is therefore limited to the melt and crystal domain. The 3D radiative heat transfer between all radiative elements within the furnace is precisely calculated by taking into account all visible and hidden objects in the furnace with a view and hidden algorithm proposed by Dupret et al. (1990). Temperature continuity and heat balance conditions are ensured at all radiative surfaces and conductive interfaces between two block regions.

The global solution is obtained by an iterative procedure that consists of a set of local iterations for each block and the calculation of radiative heat transfer in the furnace (for additional details, see Liu and Kakimoto, 2005). Moreover, a global conjugated iteration among them through iteratively updates the thermal field on all radiative surfaces and conductive interfaces between two regions. The thermal fields in all constituents and different forms of heat transfer in the furnace are thus coupled. The crystal growth rate and the crystal radius are set as parameters of the computation. The heater power is an unknown a priori. It is obtained by iterative adjustments until the temperature at the tri-junction approaches the melting point of silicon. Position of the melt-crystal interface is obtained by iterative modifications until it approaches the melting isotherm of silicon. For details of the model, the reader may consider Liu and Kakimoto (2005), who developed a general 3D global model suitable for 3D global modeling as well as 2D global modeling.

### 3 Model description

The schematic of the small CZ furnace considered in this study is illustrated in Fig. 1. As anticipated, in this study, the 3D domain (shadowed in Fig. 1) includes the crystal, melt, crucible and heater. The other regions in the

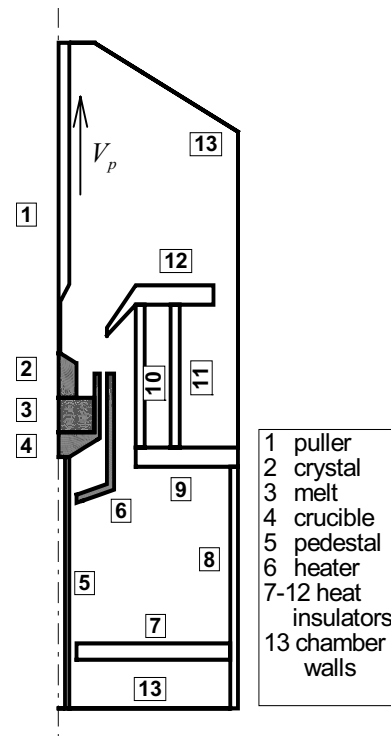


Figure 1 : Schematic of a growth furnace

furnace are included in the 2D domain. A local view of the computation grid system is shown in Fig. 2. The calculation of view factors in the radiation modeling is an important part of the model with such a space discretization scheme. Let  $\partial V^2$  and  $\partial V^3$  respectively denote the radiative surfaces that fall in the 2D domain and 3D domain of a furnace. For any two radiative surface elements  $X$  and  $X_i$ , the view factor  $K_e(X, X_i)$  between them is deduced and calculated as follows:

when  $X_i \in \partial V^2$ ,

$$K_e(X, X_i) = K_C(\vec{x}_c, \vec{x}_{ic}), \tag{1}$$

when  $X_i \in \partial V^3$  and  $X \in \partial V^2$ ,

$$K_e(X, X_i) = \frac{(\theta_{i2} - \theta_{i1})}{2\pi} K_C(\vec{x}_c, \vec{x}_{ic}), \tag{2}$$

when  $X_i \in \partial V^3$  and  $X \in \partial V^3$ ,

$$K_e(X, X_i) = \int_{\theta_{i1}}^{\theta_{i2}} K(\vec{x}_c, \vec{x}_i^*) d\theta^*, \tag{3}$$

where  $\vec{x}_c$  and  $\vec{x}_{ic}$  are the respective circumferential projections in a meridional plane of the geometrical centers of  $X$  and  $X_i$ . Azimuthal angle range  $(\theta_{i1}, \theta_{i2})$  is

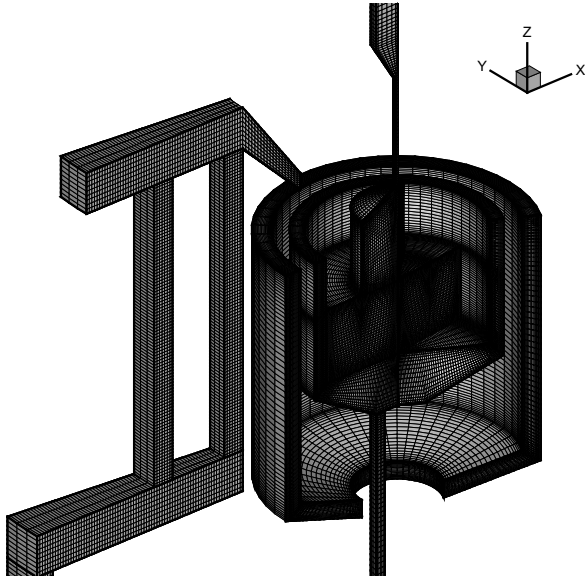


**Figure 2** : A local view of the mesh in the furnace

covered by the radiative surface element  $X_i \in \partial V^3$  and  $\vec{x}_i^* = (r'_{ic} \cos \theta^*, r'_{ic} \sin \theta^*, z'_{ic})$ . The axisymmetric view factor  $K_C(\vec{x}'_c, \vec{x}'_{ic})$  is defined by the integral

$$K_C(\vec{x}'_c, \vec{x}'_{ic}) = \int_0^{2\pi} K(\vec{x}'_c, \vec{x}'_i) d\theta^* \quad (4)$$

As mentioned in the introduction, it is precisely calculated by taking into account all objects in view and all hidden objects in the furnace with a view and hidden algorithm [Dupret et al. (1990)].

Transverse magnetic fields influence interface shape and temperature distribution near the melt-crystal interface through melt convection in the crucible via the Lorentz force. The governing equations for melt convection under the influence of a transverse magnetic field with the assumptions of a quasi-steady process and incompressible laminar flow of the melt can be written as follows:

$$\nabla \cdot \vec{V} = 0, \quad (5)$$

$$\rho \vec{V} \cdot \nabla \vec{V} = -\nabla p + \nabla \cdot \left[ \mu \left( \nabla \vec{V} + \nabla \vec{V}^T \right) \right] - \rho \vec{g} \beta_T (T - T_m) + \vec{J} \times \vec{B}, \quad (6)$$

$$\rho c \vec{V} \cdot \nabla T = \nabla \cdot (k \nabla T), \quad (7)$$

where  $\vec{V}$ ,  $\rho$ ,  $p$ ,  $\mu$ ,  $\vec{g}$ ,  $\beta_T$ ,  $\vec{J}$ ,  $\vec{B}$ ,  $c$  and  $k$  are melt velocity, melt density, melt pressure, melt viscosity, gravita-

tional acceleration, thermal expansion coefficient, electrical current density, magnetic flux density, heat capacity and thermal conductivity, respectively.

In order to obtain the Lorentz force in the melt, we need to solve the electrical field induced by the imposed magnetic field. Such phenomenon is governed by the following equations [Ozoe and Iwamoto (1994)]:

$$\nabla \cdot \vec{J} = 0, \quad (8)$$

$$\vec{J} = \sigma \left( \vec{E} + \vec{V} \times \vec{B} \right), \quad (9)$$

$$\vec{E} = -\nabla \psi, \quad (10)$$

where  $\sigma$ ,  $\vec{E}$  and  $\psi$  are electrical conductivities, electric field and electric potential, respectively. The melt flow is solved by a finite volume method.

## 4 Results

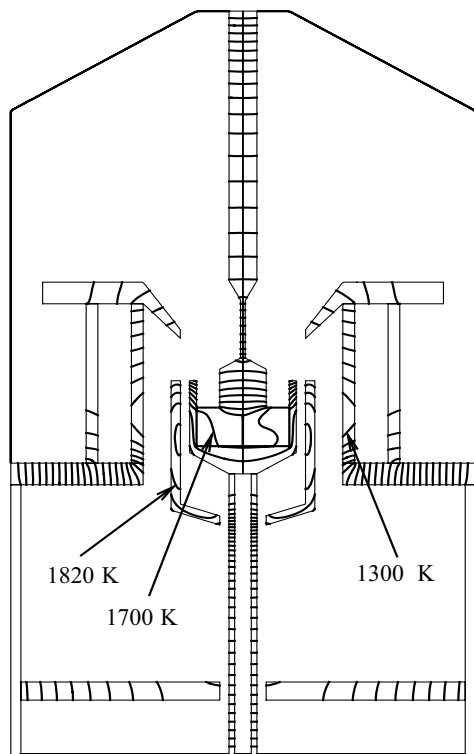
The diameters of the crystal and crucible are 32 mm and 64 mm, respectively. The depth of the melt is 28 mm. The properties of the constituent materials of the furnace are listed elsewhere [Liu and Kakimoto (2005)]. The 3D domain in this system is composed of 364,500 control volumes and 22,400 radiative surface elements, while the discrete system in the 2D domain is composed of 6,170 control volumes and 1,609 radiative surface elements.

Figure 3 shows temperature distributions in symmetric planes parallel and perpendicular to the transverse magnetic field. The intensity of the magnetic field is 0.1 T, applied in the x-direction in Fig. 2. The isotherms are plotted with increments of 40K. It can be noted that the distribution of temperature inside the melt is asymmetric. Such asymmetric distribution depends on the non-axisymmetric effect of the applied transverse magnetic field.

Figure 4 shows the 3D distribution of temperature in the crystal, the melt, the crucible and the heater. This figure illustrates in detail how the thermal field in the central regions of the furnace has a 3D structure, especially in the melt.

An area with low temperature is established along the x-direction at the top of the melt. Such asymmetric temperature profile penetrates in the bottom of the melt due to the effect of the flow.

The melt-crystal interface also has a 3D shape (elliptic shape, as shown in Fig. 5, in which the direction of the



**Figure 3 :** Isotherms in planes parallel to (left half-plane) and perpendicular to (right half-plane) the magnetic field.

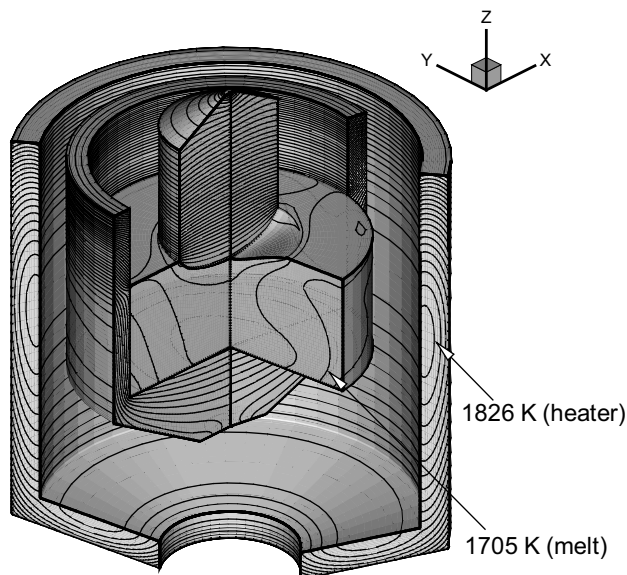


**Figure 4 :** 3D temperature distribution in the crystal, melt, crucible and heater. Isotherms are plotted with temperature increments of 7.5 K.

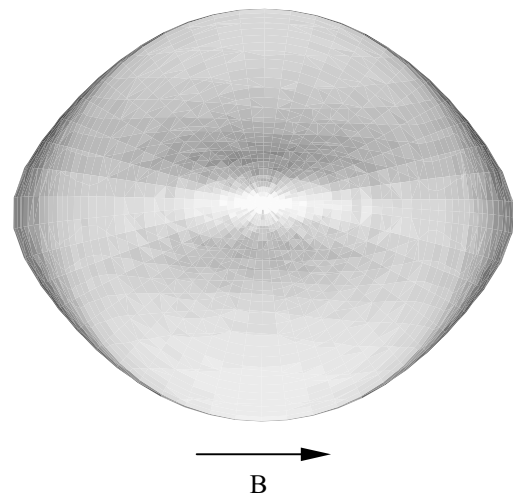


**Figure 5 :** Three-dimensional shape of the interface between solid and melt under transverse magnetic fields (no rotation of crystal and crucible).

magnetic field is indicated). Since both the crystal and the crucible were stopped in this calculation (no rotation), this elliptic shape is the consequence of the flow structure induced by the transverse magnetic field, which is unidirectional. It is worth noting that such a shape has been found experimentally in the case of crystal growth of GaAs by Kajigaya et al. (1991).

In practice, heat and mass transfer in the y-direction (perpendicular to the magnetic field) are not effectively suppressed by the transverse magnetic field, while it effectively suppresses flow in planes parallel to its direction. Figure 6 shows the azimuthal temperature distributions at some representative locations respectively on the crystal sidewall, melt surface, crucible inside and outside walls. Even on the crucible outside wall, the temperature difference in the azimuthal direction is 5 K. This demonstrates that a 3D global modeling is necessary. The converged value of the input heater power is 16.0 kW for this case.

Figures 7, 8 and 9 provide additional insights into the physics of the problem and related numerical results.

The numerical simulations also prove (not shown) that the inhomogeneity in the azimuthal direction is damped when rotation of crystal and crucible is considered.

Figure 7 shows a schematic diagram of electric current and Lorentz force at the initial stage of application of the transverse magnetic fields to the melt. An electric current induced by the magnetic field can flow in a direction par-

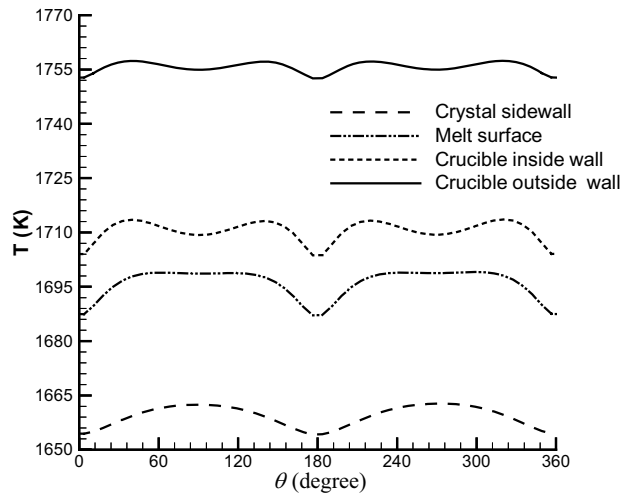


**Figure 6 :** Azimuthal temperature distributions at some representative locations respectively on the crystal sidewall, melt surface, crucible inside and outside walls.

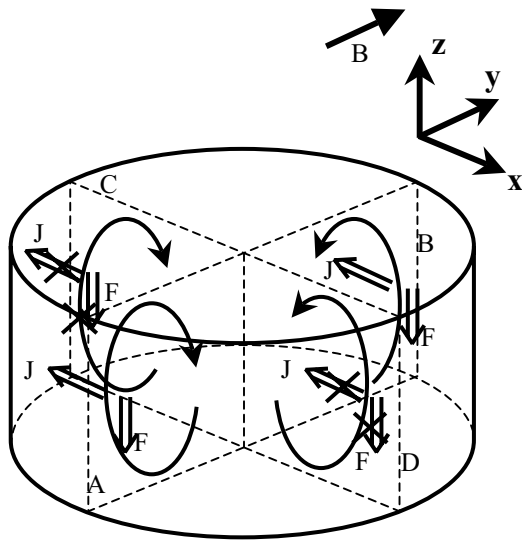


**Figure 7 :** A schematic diagram of electric current and Lorentz force at the initial stage of application of transverse magnetic fields to the melt.

allel to the crucible wall at positions A and B in the figure. Therefore, the melt motion is effectively suppressed by the Lorentz force [Kakimoto and Ozoe (2000)].

The situation regarding current flow and Lorentz force at positions C and D is the opposite to that of the above case. The electric current near the wall at positions C and D cannot flow into or from the electrically insulated wall. Therefore, the Lorentz force vanishes at these positions.

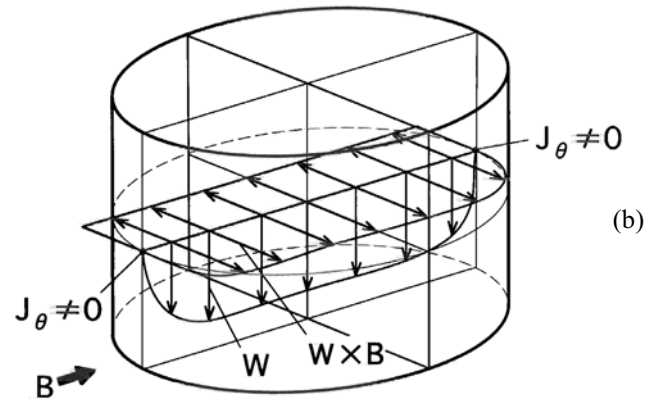
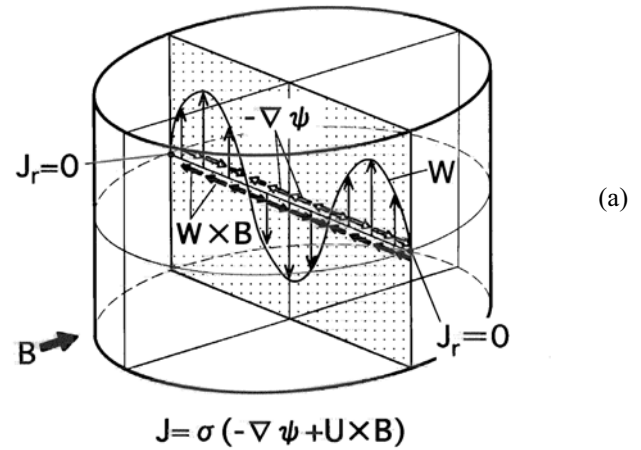


**Figure 8 :** A schematic diagram of electric current and Lorentz force in the melt under transverse magnetic fields.

Consequently, the melt motion cannot effectively be suppressed as shown in Fig. 8(a). In this figure  $U$ ,  $W$  and  $\Psi$  represent velocity, velocity in the  $z$ -direction and electric potential, respectively. Only a downward flow remains in the  $y$ - $z$  plane, while natural convection still exists in the  $x$ - $z$  plane as shown in Fig. 8(b). According to the above arguments, two main rolls aligned along the  $x$  direction exist and effectively affect heat and mass flow. This means that the heat transfer in the melt in the  $x$  direction is larger than that in the  $y$  direction; therefore, an asymmetric temperature profile is formed in the melt.

Time-dependent calculation of such temperature and velocity distributions in the melt shows that these asymmetric profiles are fixed in a laboratory frame except for a layer close to the crucible wall.

Fig. 9(a) shows temperature distribution at the top of the melt, and Figs. 9 (b), and (c) show velocity distributions in the meridian plane along the magnetic field, and in

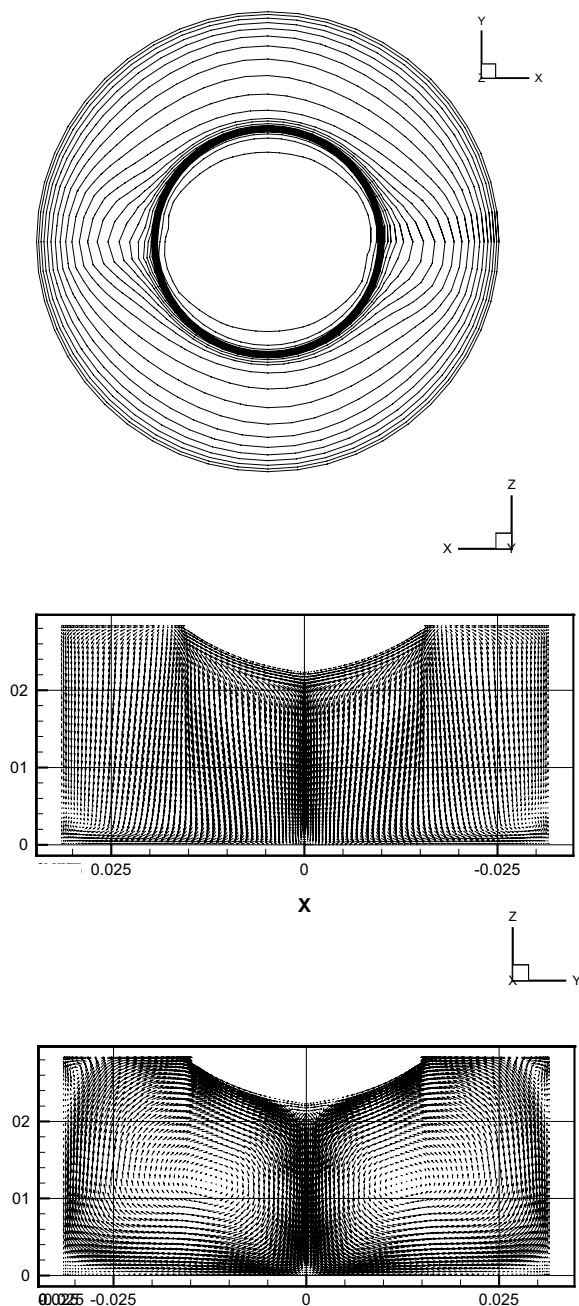


**Figure 9** : Temperature distribution at the top of the melt under transverse magnetic fields (a), velocity distribution in a meridian plane parallel (b) and perpendicular (c) to the fields.

the meridian plane perpendicular to the magnetic field, respectively.

An elliptic temperature distribution due to inhomogeneous heat transfer in the melt can be seen in Fig. 9

(a). As schematically shown in Figs. 9 (b) and (c), only a down-flow occurs in a plane parallel to the magnetic field, while two roll cells are formed in a plane perpendicular to the field. Consequently, thin boundary layers of velocity, temperature and oxygen near the crucible wall are formed.

(a) This phenomenon is a characteristic of a transverse magnetic field, which is static and non-axisymmetric. If an axisymmetric magnetic field such as a vertical or a cusp-shaped field is used, the melt rotates with the same angular velocity of the crucible.

## 5 Conclusions

Magnetic fields can stabilize unstable flow in a crucible. Diameter of crystals are increasing due to the requirement of electronic devices, therefore the diameter of melt zones is also going to increase. Magnetic-field-applied crystal growth is going to be a powerful tool to control instability of the melt.

(b) In this analysis the effect of a transverse magnetic field has been evaluated by direct numerical simulation. It has been shown that 3D flow modeling is a necessary prerequisite for a correct investigation of the problem. Some insights into the 3D structure of the flow in a realistic Czochralski configuration have been provided together with a related explanation in terms of magnetic field effects.

(c) **Acknowledgement:** This work was supported by a NEDO project, a Grant-in-Aid for Scientific Research (B) 14350010 and a grant-in-aid for the creation of innovation through business-academy-public sector cooperation from the Japanese Ministry of Education, Science, Sports and Culture.

## References

- Amberg, G. and Shiomi, J.** (2005): Thermocapillary flow and phase change in some widespread materials processes. *FDMP: Fluid Dynamics & Materials Processing*, vol 1, pp. 81-95.
- Dupret, F.; Nicodeme, P.; Ryckmans, Y.; Wouters, P.; Crochet, M.** (1990): Global Modeling Of Heat-Transfer In Crystal-Growth Furnaces, *Int. J. Heat Mass Transfer*, vol. 33, pp. 1849-1871.
- Gelfgat A. Yu., Rubinov A., Bar-Yoseph P.Z. and**

- Solan A.** (2005): On the Three-Dimensional Instability of Thermocapillary Convection in Arbitrarily Heated Floating Zones in Microgravity Environment , *FDMP: Fluid Dynamics & Materials Processing*, Vol. 1, No.1, pp 21-32
- Grabner, O.; Mueller, G.; Tomzig, E.; Von, Ammon, W.** (2001): Effects of various magnetic field configurations on temperature distributions in Czochralski silicon melts, *Microelectronic Engineering*, vol. 56 pp. 83-92.
- Hirata, H.; Hoshikawa, K.** (1989): Homogeneous Increase In Oxygen Concentration In Czochralski Silicon-Crystals By A Cusp Magnetic-Field, *J Crystal Growth*, vol. 96, pp. 747-751.
- Jaber T. J. and Saghir M. Z.** (2006), The Effect of Rotating Magnetic Fields on the Growth of SiGe Using the Traveling Solvent Method, *FDMP: Fluid Dynamics and Materials Processing*, Vol. 2, No. 3, pp. 175-190.
- Kajigaya T.; Kimura T.; Kadota Y.** (1991): Effect of the magnetic flux direction on LEC GaAs growth under magnetic field, *J. Crystal Growth*, vol. 112, pp. 123-128.
- Kakimoto, K.; Yi, K.Y.; Eguchi, M.** (1996): Asymmetric distribution of oxygen concentration in the Si melt of a Czochralski system, *J. Crystal Growth*, vol. 163, pp. 238-243.
- Kakimoto, K.** (2002): Effects of rotating magnetic fields on temperature and oxygen distributions in silicon melt, *J. Crystal Growth*, vol. 237-239, pp. 1785-1790.
- Kakimoto, K.; Tashiro, A.; Shinozaki, T.; Ishii, H.; Hashimoto, Y.** (2002): Mechanisms of heat and oxygen transfer in silicon melt in an electromagnetic Czochralski system, *J. Crystal Growth*, vol. 243, pp. 55-65.
- Kakimoto, K.; Ozoe, H.** (2000): Oxygen distribution at a solid-liquid interface of silicon under transverse magnetic fields, *J. Crystal Growth*, vol. 212, pp. 429-437.
- Krauze, A.; Muiznieks, A.; Muhlbauer, A.; Wetzel, T.; Gorbunov, L.; Pedchenko, A.; Virbulis, J.** (2004): modelling of turbulent melt flow in large CZ system with horizontal DC magnetic field-I: flow structure analysis, *J. Crystal Growth*, vol. 262, pp. 157-162.
- Lan C. W.; Yeh B.C.** (2005): Effects of Rotation on Heat Flow, Segregation, and Zone Shape in a Small-scale Floating-zone Silicon Growth under Axial and Transversal Magnetic Fields, *FDMP: Fluid Dynamics and Materials Processing*, vol. 1, No. 1, pp. 33-44.
- Lappa M.** (2005): Review: Possible strategies for the control and stabilization of Marangoni flow in laterally heated floating zones, *FDMP: Fluid Dynamics and Materials Processing*, Vol. 1, No.2, pp. 171-188.
- Li Y. R.; Peng L.; Shi W. Y.; Imaishi N.** (2006): Convective instability in annular pools, *FDMP: Fluid Dynamics and Materials Processing*, Vol. 2, No. 3, pp. 153-166.
- Liu, L.; Kakimoto, K.** (2005a): Partly three-dimensional global modeling of a silicon Czochralski furnace. I. Principles, formulation and implementation of the model, *Int. J. Heat Mass Transfer*, vol. 48 (21-22), pp. 4481-4491.
- Liu, L.; Kakimoto, K.** (2005b): Partly three-dimensional global modeling of a silicon Czochralski furnace. II. Model application: Analysis of a silicon Czochralski furnace in a transverse magnetic field, *Int. J. Heat Mass Transfer*, vol. 48 (21-22), pp. 4492-4497.
- Liu, L.; Nakano, S.; Kakimoto, K.** (2005): An analysis of temperature distribution near the melt-crystal interface in silicon Czochralski growth with a transverse magnetic field, *J. Crystal Growth*, vol. 282 (1-2), pp. 49-59.
- Ozoe, H.; Iwamoto, M.** (1994): COMBINED EFFECTS OF CRUCIBLE ROTATION AND HORIZONTAL MAGNETIC-FIELD ON DOPANT CONCENTRATION IN A CZOCHRALSKI MELT, *J. Crystal Growth*, vol. 142, pp. 236-244.
- Sabhpathy, P.; Salcudean, M. E.** (1991): Numerical Study Of Czochralski Growth Of Silicon In An Axisymmetrical Magnetic-Field, *J. Crystal Growth*, vol. 113, pp. 164-172.
- Sohail M.; Saghir M. Z.** (2006), Three-Dimensional Modeling of the Effects of Misalignment on the Growth of Ge<sub>1-x</sub>Si<sub>x</sub> by The Traveling Solvent Method, *FDMP: Fluid Dynamics and Materials Processing*, Vol. 2, No. 2, pp. 127-140
- Tsukada, T.; Kobayashi, M.; Jing; C.J.; Imaishi, N.** (2005): Numerical simulation of CZ crystal growth of oxide. *FDMP: Fluid Dynamics and Materials Processing*, vol. 1(1): pp.45-62.

